RESEARCH ARTICLE

VACCINES

Genome-wide identification of interferon-sensitive mutations enables influenza vaccine design

Yushen Du,[1,2]* Li Xin,[3] Yuan Shi,[1] Tian-Hao Zhang,[1,4] Nicholas C. Wu,[4] Lei Dai,[1] Danyang Gong,[1] Gurpreet Brar,[1] Sara Shu,[1] Jiadi Luo,[1,5,6] William Reiley,[7] Yen-Wen Tseng,[1] Hongyan Bai,[3] Ting-Ting Wu,[1] Jieru Wang,[1,5] Yuelong Shu,[3,8] Ren Sun[1,2,4]*

In conventional attenuated viral vaccines, immunogenicity is often suboptimal. Here we present a systematic approach for vaccine development that eliminates interferon (IFN)–modulating functions genome-wide while maintaining virus replication fitness. We applied a quantitative high-throughput genomics system to influenza A virus that simultaneously measured the replication fitness and IFN sensitivity of mutations across the entire genome. By incorporating eight IFN-sensitive mutations, we generated a hyper–interferon-sensitive (HIS) virus as a vaccine candidate. HIS virus is highly attenuated in IFN-competent hosts but able to induce transient IFN responses, elicits robust humoral and cellular immune responses, and provides protection against homologous and heterologous viral challenges. Our approach, which attenuates the virus and promotes immune responses concurrently, is broadly applicable for vaccine development against other pathogens.

Most viruses adapt rapidly to diverse selection pressures, posing a challenge for deploying safe and effective vaccines. Influenza viruses, for example, are characterized by large genetic diversity across subtypes and rapid antigenic drift and shift, which present problems for traditional vaccine strategies. Attenuation or inactivation of viruses tends to reduce the strength and breadth of immune responses, resulting in ineffective protection against antigenic alterations (*1*–*3*). Previous pandemics and recent influenza outbreaks highlight the need to develop safe vaccines that elicit effective immune responses and confer broad protection.

The type I interferon (IFN) system is the major component of innate immune responses (*4*–*6*). The IFN response provides the first line of defense against viral infections by inducing the expression of hundreds of IFN-stimulated genes (ISGs), many of which have antiviral activities (*7*). The IFN response is also critical for dendritic cell maturation, development of B and T cells, and memory formation, bridging innate and adaptive immunity (*8*–*12*). Most viruses have evolved to efficiently suppress the production and function of IFN to allow replication in vivo. Thus, systematic elimination of IFN-modulating functions from the virus presents a potential approach for vaccine development (fig. S1) (*13*, *14*). Removing the most well-characterized IFN modulator in influenza virus—namely, the NS1 protein—has shown promise in a vaccine candidate (delNS1) in phase 1/2 clinical trials (*14*, *15*). Although studies have suggested that influenza proteins other than NS1 have IFN-modulating functions (*16*, *17*), genome-wide identification and elimination of IFN-modulating functions without affecting viral replication fitness in vitro have remained challenging tasks.

To tackle this challenge, we developed a quantitative high-throughput genomics system, which combines saturation mutagenesis and next-generation sequencing, to comprehensively identify IFN-modulating functions in the entire viral genome (*18*). This system has enabled us to quantitatively measure the replication capacity of a large number of mutants in parallel under specific conditions (*18*, *19*). We performed comparative profiling of the entire influenza genome with and without IFN selection, which led to the identification of IFN-modulating functions on multiple viral segments. By combining eight IFN-sensitive mutations across the viral genome, we generated a hyper–interferon-sensitive (HIS) virus that is replication-competent in vitro but highly attenuated in IFN-competent hosts in vivo. The HIS virus showed desired properties as a safe and effective live attenuated influenza vaccine with robust humoral and cellular responses, and it provided broad protection against homologous and heterologous viral challenges in mice and ferrets.

Fitness profile of the influenza A viral genome at single-nucleotide resolution

The eight-plasmid reverse genetic system carrying the influenza A/WSN/33 (H1N1) virus genome was used for the construction of mutant plasmid libraries (*20*). The mutants were divided into 52 sublibraries, each of which contained single-nucleotide mutations in a small genome region of 240 base pairs that were generated by error-prone polymerase chain reaction (fig. S2) (*21*–*23*). Viral mutant libraries were reconstituted in human embryonic kidney 293T cells by cotransfecting the plasmid encoding the sublibrary of mutants with the other seven plasmids encoding wild-type (WT) viral proteins. To systematically identify IFN-modulating functions, all viral libraries were selected in A549 cells with or without exogenous IFN treatment (IFN-α_2 at inhibitory concentration 80) (*19*). Illumina sequencing was used to identify each mutant and to calculate the corresponding frequency within each sublibrary. The relative fitness (RF) score of a mutant virus was calculated as the ratio of the relative frequency in the selected virus library to that in the plasmid library (Fig. 1A and table S1). There were strong correlations between biological duplicates of transfection and of selection (fig. S3). We observed a clear separation of the distribution of fitness effects between synonymous mutations and nonsense mutations (fig. S4A), indicating effective selection on virus mutants. To further validate the accuracy of the fitness profiling, we randomly selected 26 missense mutations and characterized the corresponding mutant viruses individually. The replication capacity of each mutant was highly correlated with the RF scores from the fitness profiling (fig. S4B). Using synonymous mutations as a benchmark, 50.7% of missense mutations across the whole genome were deleterious, in accordance with previous findings that single mutations are poorly tolerated in the genomes of RNA viruses (fig. S5A) (*24*, *25*).

Systematic identification of IFN-sensitive mutations

The RF scores of most mutants are correlated in the presence and absence of exogenous IFN treatment; however, we observed a set of mutations that were nearly neutral in the absence of IFN but highly deleterious under IFN selection (Fig. 1B and fig. S6). These putative IFN-sensitive mutations were widespread on multiple viral segments. Among all influenza A viral proteins, NS1 has been extensively studied for its interaction with the IFN pathway (*19*, *26*, *27*), which is validated both in our fitness profiling and individually constructed NS1 mutant viruses (fig. S7).

[1]Department of Molecular and Medical Pharmacology, University of California, Los Angeles, CA 90095, USA. [2]Cancer Institute, Collaborative Innovation Center for Diagnosis and Treatment of Infectious Diseases, School of Medicine, Zhejiang University, Hangzhou 310058, China. [3]National Institute for Viral Disease Control and Prevention, Collaborative Innovation Center for Diagnosis and Treatment of Infectious Diseases, Chinese Center for Disease Control and Prevention, Key Laboratory for Medical Virology and Viral Diseases, Ministry of Health of the People's Republic of China, Beijing 102206, China. [4]Molecular Biology Institute, University of California, Los Angeles, CA 90095, USA. [5]Department of Pediatrics, University of Pittsburgh School of Medicine, Pittsburgh, PA 15224, USA. [6]Department of Pathology, The Second Xiangya Hospital of Central South University, Changsha, Hunan 410005, China. [7]Trudeau Institute, Saranac Lake, NY 12983, USA. [8]School of Public Health (Shenzhen), Sun Yat-sen University, Guangdong 510275, China.
***Corresponding author. Email: lily.duyushen@gmail.com (Y.D.); rsun@mednet.ucla.edu (R.S.)**

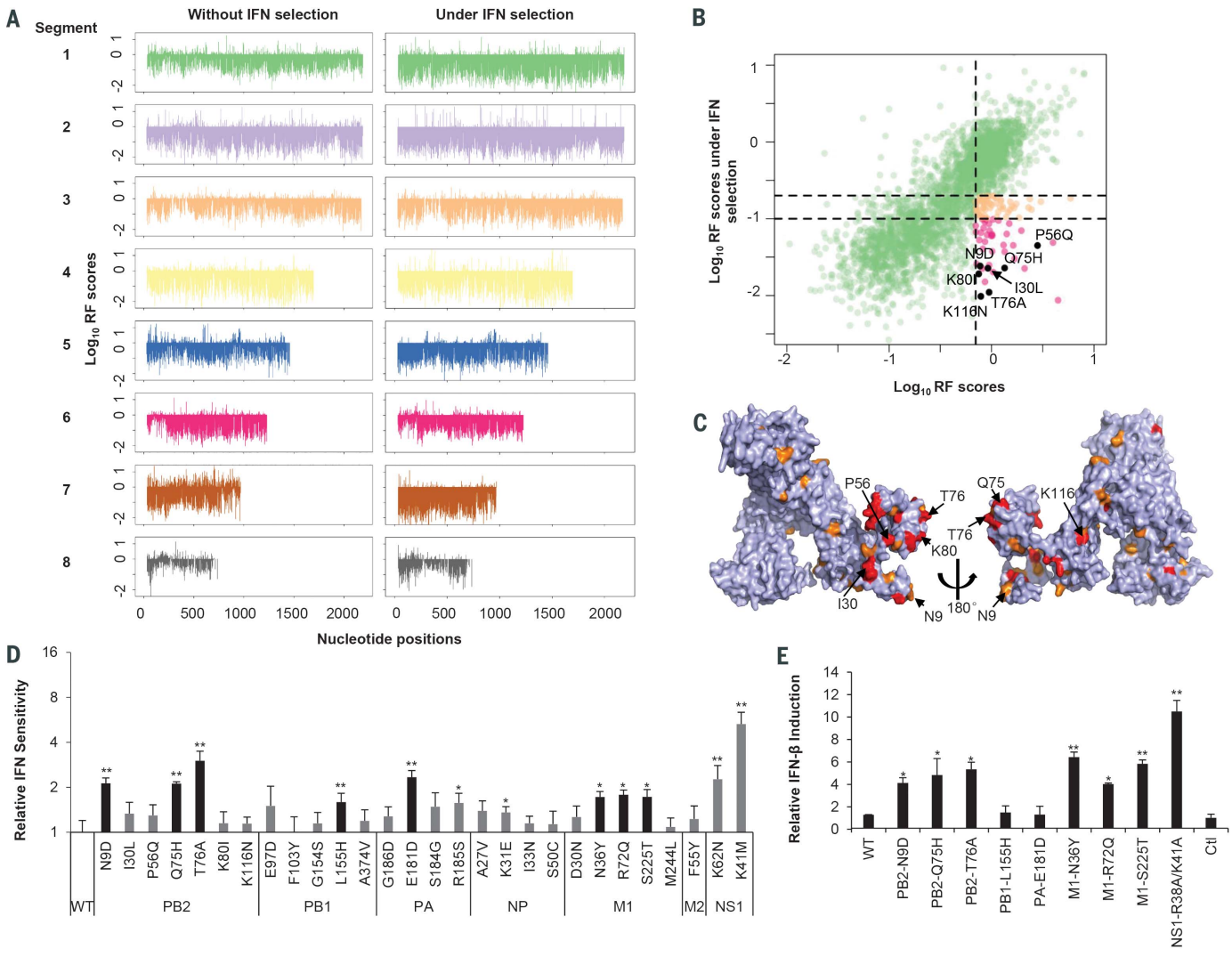

Fig. 1. Identification of IFN-sensitive mutations using quantitative high-throughput genomics. (**A**) Relative fitness (RF) scores for individual mutations in A549 cells with (right) and without (left) IFN selection across the influenza A/WSN/33 genome. (**B** and **C**) Identification of IFN-sensitive mutations with PB2 protein as an example [Protein Data Bank (PDB) ID, 4WSB] (*38*, *39*). Red and orange represent strong and intermediate IFN sensitivity, respectively. (**D**) Validation of IFN sensitivity with individually reconstituted mutants (n = 4). The top eight mutations on nonsurface virion proteins are shown in black. (**E**) Induction of IFN-β expression in A549 cells infected with WT virus or indicated mutants at 6 hours post-infection, with mock infection as control (Ctl) (n = 3). Error bars, SD. *P < 0.05, **P < 0.01 [two-tailed t test compared with WT (D) or with Ctl (E)]. Single-letter abbreviations for the amino acid residues are as follows: A, Ala; C, Cys; D, Asp; E, Glu; F, Phe; G, Gly; H, His; I, Ile; K, Lys; L, Leu; M, Met; N, Asn; P, Pro; Q, Gln; R, Arg; S, Ser; T, Thr; V, Val; W, Trp; and Y, Tyr.

To further explore IFN-modulating functions across the genome, we focused on IFN-sensitive mutations outside NS1, especially the solvent-exposed and structurally clustered residues in the polymerase complex (PB2, PB1, PA, and NP), as well as the M1 and M2 proteins (Fig. 1C and fig. S6). Twenty-six mutations were constructed individually, most of which were nearly neutral for viral replication with nearly intact polymerase activity (fig. S8). These included the previously characterized mutations PB2-N9D, which is known to counteract the inhibition of MAVS (mitochondrial antiviral signaling protein)–induced IFN-β production by PB2 (*16*), and M1-D30N, which has been shown to induce IFN-β production (*17*). Several mutations significantly increased IFN sensitivity compared with WT, and the top eight were chosen for further characterization (Fig. 1D). Six of them (PB2-N9D, PB2-Q75H, PB2-T76A, M1-N36Y, M1-R72Q, and M1-S225T) elevated the expression of IFN-β and ISG54 (Fig. 1E and fig. S9) and stimulated nuclear translocation of IRF3 (fig. S10). We also observed that the IFN induction was MAVS-dependent and STING (stimulator of interferon genes)–independent (fig. S11). Moreover, these six mutants were not sensitive to IFN treatment in Vero cells, which are deficient in IFN production. However, the other two mutations (PB1-L155H and PA-E181D) did not induce higher IFN production (Fig. 1E) and were still IFN-sensitive in Vero cells, suggesting that these mutants likely affect processes downstream of IFN production.

Combining mutations increases IFN sensitivity and IFN induction in vitro

To maximize IFN sensitivity and IFN induction, we combined three IFN-inducing mutations on PB2 (N9D, Q75H, and T76A), three on M1 (N36Y, R72Q, and S225T), and two previously reported ones on NS1 (R38A and K41A) to create the HIS virus. The growth of HIS virus in IFN-competent A549 cells showed significant attenuation compared

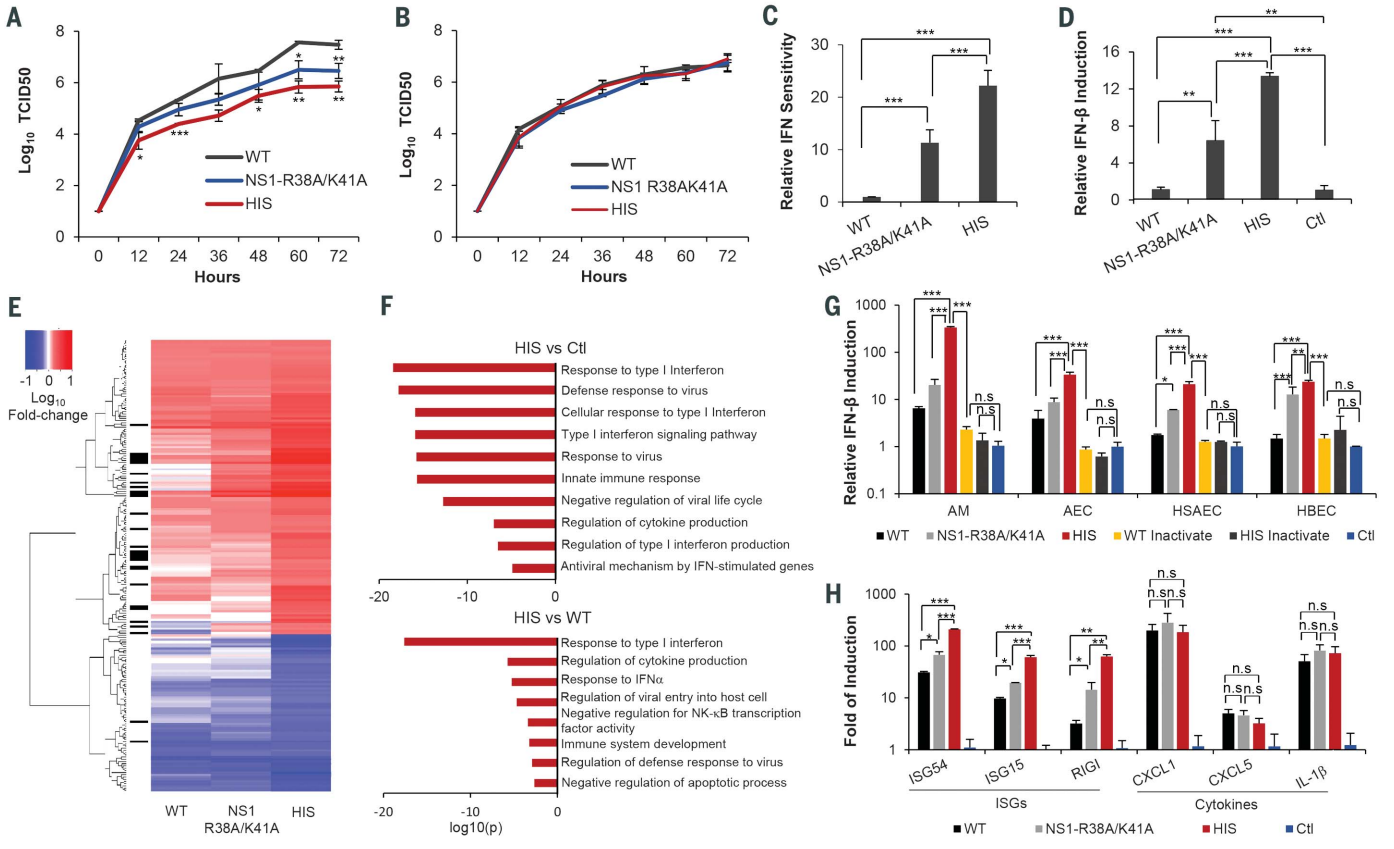

Fig. 2. The combination of mutations in HIS virus increases IFN sensitivity and IFN production. (**A** and **B**) Replication kinetics of WT, NS1 mutant, and HIS viruses in A549 (A) and Vero (B) cells. (**C**) IFN sensitivity of WT, NS1 mutant, and HIS viruses ($n = 4$). (**D**) Induction of IFN-β expression by indicated virus in A549 cells at 6 hours post-infection, with mock infection as Ctl ($n = 3$). (**E**) Global gene expression in A549 cells infected with indicated viruses was examined by RNA sequencing ($n = 2$). The heatmap shows the genes that were significantly differentially expressed in HIS-infected cells compared with mock-infected cells. IFN response genes are marked on the left with black bars. (**F**) GO enrichment analysis of genes up-regulated in HIS-infected cells in comparison with mock- (top) or WT-infected (bottom) cells. (**G**) Induction of IFN-β expression by indicated viruses in primary human alveolar macrophages (AMs), human alveolar epithelial cells (AECs), human small airway epithelial cells (HSAECs), and human bronchial epithelial cells (HBECs) at 6 hours post-infection, with mock infection as Ctl ($n = 3$). (**H**) Induction of indicated ISGs and inflammatory cytokines in primary human AMs at 6 hours post-infection ($n = 3$). Error bars, SD. $^*P < 0.05$, $^{**}P < 0.01$, $^{***}P < 0.001$ [one-way analysis of variance (ANOVA) with Bonferroni multiple comparisons test]; n.s, not significant.

with that of WT virus (1.4-log decrease at 36 hours and 1.8-log decrease at 60 hours) but was fully restored in IFN-deficient Vero cells (Fig. 2, A and B). The IFN sensitivity of HIS virus was significantly higher than that of the NS1-R38A/K41A mutant, indicating an independent effect of mutations on PB2 and M1 (Fig. 2C). Gene expression data from lung epithelial and macrophage cell lines (A549 and THP1) showed that HIS virus induced higher IFN production and responses (Fig. 2D and fig. S12, A to C). Using RNA sequencing, we evaluated the global gene expression changes in A549 cells infected with WT, NS1-R38A/K41A, or HIS virus. At 6 hours post-infection, the expression of 120 genes was significantly up-regulated (fold change > 2 and $P < 0.001$) in HIS-infected cells, of which 24% were IFN response genes (Fig. 2E, fig. S12D, and table S2). Gene Ontology (GO) enrichment analysis revealed that the pathways related to IFN production and response were the dominant ones activated by HIS virus, to a greater extent than by WT or mock infection (Fig. 2F). Furthermore, HIS virus induced negative regulators of apoptosis process, such as TNFAIP3, an important inhibitor of TNF-mediated apoptosis. Slower cell death was observed with HIS infection than with WT infection (fig. S12E).

We further defined the phenotypes of HIS virus with a panel of human lung cells, including immortalized small airway epithelial cells, bronchial epithelial cells, primary alveolar epithelial cells, and primary alveolar macrophages (Fig. 2G). HIS virus induced the strongest up-regulation of IFN-β expression (~50-fold relative to WT) in the primary alveolar macrophages, an important target for influenza infection (Fig. 2G), and greater up-regulation of ISGs than WT virus (Fig. 2F). HIS virus did not enhance the expression of other inflammatory cytokines [CXCL1, CXCL5, or interleukin-1β (IL-1β)] in the infected macrophages, highlighting its specific effects on the IFN pathway (Fig. 2H). The phenotype of HIS virus is not limited to the WSN background: Introducing these eight mutations into another H1N1 strain of influenza, A/PR8/34 (PR8-HIS), led to a similar phenotype (fig. S12, F and G). The up-regulation of the IFN pathway requires active viral infection, given that formalin-inactivated HIS virus lost the ability to induce higher IFN-β expression (Fig. 2G).

HIS virus is highly attenuated in IFN-competent mice and ferrets

We next measured the replication and pathogenesis of HIS virus in mice and ferrets, the most commonly used animal models for influenza virus. BALB/c mice were intranasally inoculated with WT or HIS virus at different doses. Whereas the median lethal dose of WT virus was 5×10^5 TCID50 (50% tissue culture infective dose), and 1×10^3 TCID50 caused obvious body weight loss in all animals, neither weight loss nor indicative clinical symptoms were observed in HIS-infected mice given 1×10^7 TCID50, the highest dose that we have tested (Fig. 3, A and B). To compare the HIS

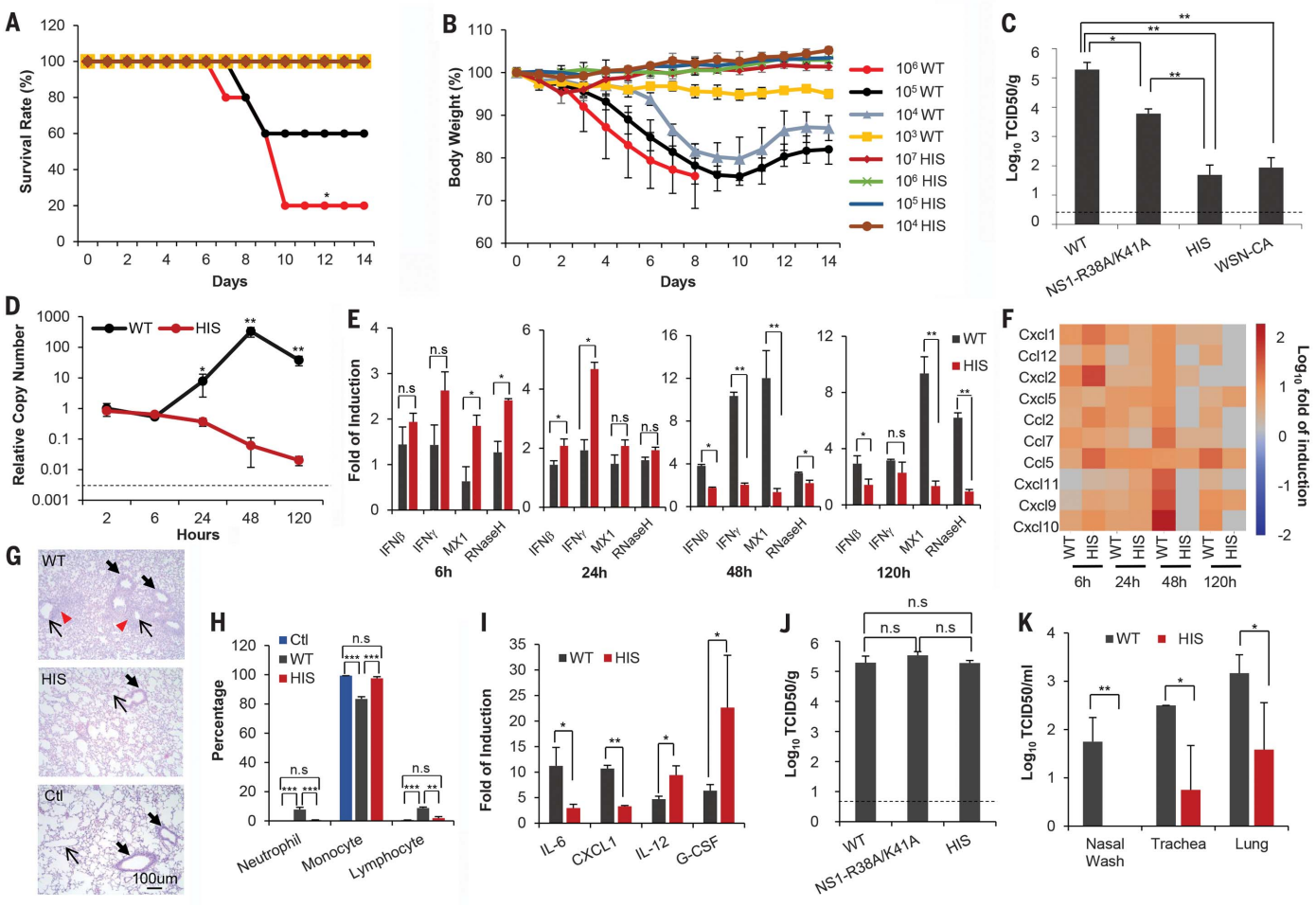

Fig. 3. HIS virus is replication-deficient in vivo and induces a transient IFN response. (**A** and **B**) Survival rate and percentage of body weight loss after intranasal infection (n = 5). (**C** and **D**) Viral titers at day 2 post-infection (n = 4) (C) and replication kinetics (n = 3) (D) of WT and HIS viruses in mouse lung tissues. (**E**) Induction of indicated ISGs in mouse lung tissues at 6, 24, 48, and 120 hours (h) post-infection (n = 3), shown as fold of induction over mock infection. RNase H, ribonuclease H. (**F**) Gene expression of indicated inflammatory cytokines in mouse lung tissues was examined by RNA sequencing (n = 2). (**G**) HE (hematoxylin and eosin) staining of lung tissues at day 9 post-infection. Thick arrows, bronchioles; thin arrows, vessels; red triangles, inflammatory cell infiltration. (**H**) Percentage of neutrophils, monocytes, and lymphocytes in BAL cytospins at day 9 post-infection (n = 3). (**I**) Cytokines in BAL samples measured by Luminex multiplex assay (n = 4). (**J**) Replication of indicated viruses in lung tissues of IFNAR$^{-/-}$ mice (n = 4). (**K**) Viral titer of WT and HIS viruses in ferret nasal wash, trachea, and lung tissues (n = 3). Dashed lines represent detection limits. Error bars, SD. *P < 0.05, **P < 0.01, ***P < 0.001 [log-rank test for (A); ANOVA with Bonferroni multiple comparisons test for (C), (H), and (J); and two-tailed t test for (D), (E), (I), and (K)].

virus approach with the live attenuated vaccine strategy used in FluMist, we incorporated the five cold-adapted (CA) mutations from FluMist into the WSN background and generated a WSN-CA virus (*28*, *29*). WSN-CA virus replicated well at 33°C but was highly attenuated at 39°C and induced IFN-β expression to a similar level as WT virus, which was significantly lower than that induced by HIS virus (fig. S13). By day 2 post-inoculation, replication of HIS virus in mouse lung tissues was significantly lower than that of WT virus (~3.6-log decrease) or the NS1-R38A/K41A mutant (~2-log decrease) and comparable to that of WSN-CA virus (Fig. 3C and fig. S14A). In contrast with the robust viral replication observed for WT infection, which peaked at 48 hours, no increase in viral copy number was detected in HIS-infected mice at any tested time point (Fig. 3D). PR8-HIS virus was also significantly attenuated compared with WT PR8 virus in mouse lung tissues (fig. S14B). Although highly attenuated in replication, HIS virus showed transient yet significant up-regulation of IFN and ISGs at 6 and 24 hours post-infection, after which the response was diminished (Fig. 3E). In contrast, WT virus induced a robust pro-inflammatory response throughout the course of infection, exemplified by the high induction of CXCL10 at 48 and 120 hours post-infection (Fig. 3F). These results correlate well with histological analysis of infected lungs and cytospins of bronchoalveolar lavage (BAL) fluid (Fig. 3, G and H, and fig. S14, C to G). HIS-infected lungs showed infiltration of neutrophils and lymphocytes at day 2 post-infection; however, the infiltration was transient and cleared by day 9. Sustained inflammation and tissue damage was observed for WT-infected lungs, which became more severe by day 9 post-infection (Fig. 3H and fig. S14, H and I). We also examined the cytokine response in the BAL samples at 48 hours post-infection by means of Luminex multiplex assay (Fig. 3I and fig. S14, J and K). WT infection showed significantly higher levels of IL-6 and CXCL1, consistent with the observed severe inflammation. In contrast, HIS virus induced higher amounts of IL-12 and G-CSF, which is important for granulocyte stimulation and T cell development. Furthermore, replication of HIS virus was fully restored to WT levels in IFNAR$^{-/-}$ mice, indicating that the inability to counteract IFN response was the underlying mechanism for the highly attenuated replication of HIS virus in wild-type mice (Fig. 3J). In the ferret model, we also observed significant attenuation of HIS virus (Fig. 3K). By day 3 post-infection, HIS virus showed a ~2-log decrease in trachea and a ~1.5-log decrease in lung tissues compared with WT virus. Moreover, no infectious

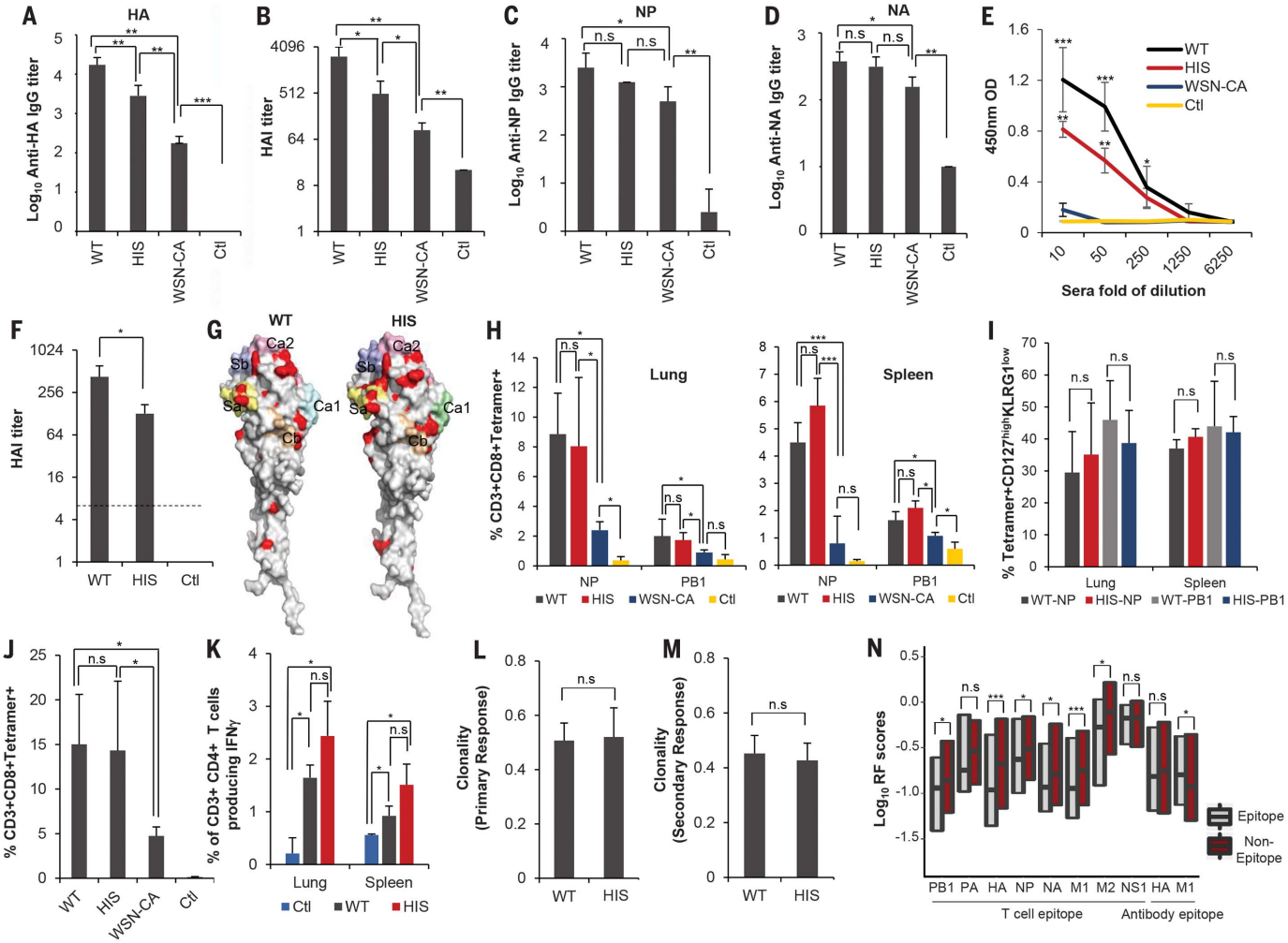

Fig. 4. HIS virus induces strong adaptive immune responses in mice and ferrets. (**A** to **D**) HA-binding IgG (n = 7), HA neutralizing antibody (n = 7), and NP- and NA-binding IgG (n = 4) in mouse sera at day 28 post-vaccination. HAI, hemagglutinin inhibition. (**E**) HA-binding IgA in BAL samples at day 28 post-vaccination (n = 4). The optical density (OD) in ELISA was 450 nm. (**F**) HA neutralizing antibody levels in ferret sera at day 22 post-vaccination (n = 3). The dashed line represents the detection limit. (**G**) Mutations not neutralized by mouse sera (red) were mapped onto the HA structure (PDB ID, 1RUZ; n = 5) (*40*). The other five colors represent five well-characterized neutralization epitopes. (**H**) Tetramer staining of antigen-specific CD8 T cells in mouse lung (left) and spleen (right) at day 10 post-vaccination (n = 10). (**I**) Percentage of antigen-specific memory precursor effector cells in mouse lung and spleen (n = 3). (**J**) NP antigen–specific CD8 T cells during the secondary responses in lung tissues from mice vaccinated with indicated viruses (n = 4). (**K**) Intracellular IFN-γ staining of CD4 T cells induced by the indicated viruses (n = 3). (**L** and **M**) Clonality of TCRβ sequences of NP antigen–specific CD8 T cells during the primary (n = 5) (L) or secondary (n = 4) (M) responses. (**N**) Box plots show the fitness distribution of mutations on T cell epitopes or antibody epitopes. Error bars, SD. *P < 0.05, **P < 0.01, ***P < 0.001 [ANOVA with Bonferroni multiple comparisons test for (A) to (D), (F), (H), (J), and (K); two-tailed t test for (I), (L), and (M); and Wilcoxon rank sum test for (N)].

viral particles were detected in nasal washes of HIS-infected ferrets, in contrast to the robust viral shedding observed during WT infection.

HIS virus induces strong and broad adaptive immune responses

We then examined the ability of the HIS virus to induce humoral and cellular responses. Mouse sera and BAL samples were collected at day 28 after single-dose (1×10^4 TCID50) vaccination with WT, HIS, or WSN-CA virus. HIS virus induced robust antibody responses, as measured by ELISA (enzyme-linked immunosorbent assay) and hemagglutinin (HA) inhibition and neutralization antibody assays (Fig. 4, A to E, and fig. S15). The level of HA antibody responses elicited by HIS virus was lower than for WT virus, yet significantly higher than for the WSN-CA, inactivated WT, and inactivated HIS viruses (Fig. 4, A and B, and fig. S15, C and D). Immunoglobulin G (IgG) antibodies against NP, NA, and M1 proteins, which have been shown to play an important role in limiting viral replication (*30*, *31*), were also detected in the sera of HIS-vaccinated mice at a level comparable to that in WT-infected mice (Fig. 4, C and D, and fig. S15E). Furthermore, mucosal immune responses, indicated by secretory IgA antibodies against HA and NP proteins, were elicited by HIS vaccination (Fig. 4E and fig. S15F). Robust HA antibody responses were also observed in ferrets vaccinated with HIS virus (Fig. 4F and fig. S15G), which were sustained for at least 50 days post-vaccination. To examine the epitope coverage of the neutralizing antibodies generated by HIS virus, we profiled the HA mutants in the presence or absence of mouse serum antibodies by using the high-throughput genomic approach (*32*). Mutations not neutralized by sera were observed in both head (Ca2 and Sa sites) and stem regions, with no significant difference in the number or the distribution of mutations between the WT and HIS viruses (Fig. 4G, fig. S16, and table S3). This suggests that the breadth and diversity of neutralizing antibodies induced by the HIS virus are comparable to those induced by the WT virus.

In addition to humoral responses, HIS virus elicited NP and PB1 antigen–specific CD8 T cell responses, similarly to WT virus and much more

strongly than the WSN-CA, inactivated WT, and inactivated HIS viruses (Fig. 4H and fig. S17, A to D). The CD8 T cells induced by the WT and HIS viruses had a similar capacity for IFN-γ production upon stimulation by viral epitope peptides (fig. S17E). We further examined the phenotypes of virus-specific T cells by quantifying the expression of KLRG1, CD127, CD44, CD62L, and CCR7. By day 21 post-infection, the NP and PB1 antigen–specific CD8 T cells induced by the WT and HIS viruses displayed similar levels of memory precursor effector cells with a $CD127^{high}KLRG1^{low}$ phenotype and short-lived effector cells with a $CD127^{low}KLRG1^{high}$ phenotype (Fig. 4I and fig. S17F). These virus-specific CD8 T cells also displayed a similar effector/memory phenotype, as measured by CD62L, CD44, and CCR7 expression (fig. S17, G and H). Consistently, after challenge infection at 1 month post-vaccination, HIS virus induced the secondary CD8 T cell responses similarly to WT but more strongly than WSN-CA virus (Fig. 4J and fig. S17I). Moreover, similar frequencies of influenza-specific CD4 T cells were elicited by the WT and HIS viruses (Fig. 4K). To examine the diversity of the primary and secondary T cell responses, we analyzed the T cell receptor repertoire by sequencing the β T cell receptor (TCRβ) loci of NP-specific CD8 T cells in mice vaccinated with WT or HIS virus. The Vβ usage and clonality for both primary and secondary T cell responses were comparable between the WT and HIS viruses, documenting the diversity of T cell lineages induced by HIS vaccination (Fig. 4, L and M, and fig. S18).

We analyzed the potential impact of immune responses on the viral genome at the population level. Our whole-genome fitness profiling provides a data set for examining the genetic flexibility of viral sequences. We calculated the fitness cost of mutations in the previously identified B and T cell epitopes. Mutations on several T cell epitopes, but not on antibody epitopes, were generally correlated with lower fitness scores (Fig. 4N and table S4). Our results suggest that an escape from T cell selection will impose a higher fitness cost for the virus, and thus T cell responses will be effective against vaccine escape.

HIS virus protects against homologous and heterologous viral challenge

We examined whether HIS vaccination could offer protection against homologous and heterologous viral challenges. Immunized mice were challenged 28 days post-vaccination with 1×10^4 TCID50 of WT virus. Vaccination by HIS virus reduced viral replication by ~3 log, with no sign of weight loss (Fig. 5 and fig. S19). Complete protection without detectable viral titers in the lung was achieved with one vaccination at a high dose (1×10^6 TCID50) or two vaccinations at a low dose (1×10^4 TCID50) (Fig. 5B and fig. S19B). Similar protective effects were observed in ferrets, which were challenged with 1×10^7 TCID50 of WT virus at day 35 post-vaccination. Nasal washes were collected at days 1, 3, 4, 7, and 9 post-challenge, and no infectious viral particles were detected in nasal washes from HIS-vaccinated ferrets throughout this time period (Fig. 5C).

To test whether HIS vaccination provides protection against heterologous strains, we first challenged immunized mice with PR8 virus and examined viral titer at day 2 post-challenge. HIS vaccination reduced viral titer by ~3 log compared with mock vaccination and significantly more than WSN-CA vaccination (fig. S19C). We further challenged vaccinated mice with a lethal dose of three different influenza strains: H1N1 subtypes A/PR8/34 and A/Cal/04/09 and H3N2 subtype A/X-31. Protection by HIS vaccination was observed in all measures, including survival rate, percentage of body weight loss, and clinical scores (Fig. 5, D and E, and fig. S19D). Strong secondary antigen-specific T cell responses were observed in the challenged mice for all strains (fig. S20). HIS vaccination also protected ferrets from heterologous A/Cal/07/09 challenge, as shown by viral titer in nasal washes and percentage of body weight loss (Fig. 5F and fig. S19E).

Discussion

Conventional approaches to develop vaccines render the virus avirulent but also reduce immunogenicity. We developed a quantitative high-throughput genomics approach to systematically identify and eliminate immune-modulating functions in the virus genome while maintaining replication fitness in vitro. This is a systems-based strategy to enhance viral immunogenicity while attenuating replication and pathogenesis. In this proof-of-principle study, we generated a HIS virus with a combination of eight IFN-sensitive mutations. These mutations also induced higher IFN production and response. We demonstrated that HIS virus is highly attenuated in vivo but is able to induce transient IFN responses, elicit robust and diverse humoral and cellular immunity, and provide protection against homologous and heterologous viral challenges in mice and ferrets.

Recent studies have suggested several strategies to design live attenuated vaccines (*14*, *15*, *33*–*37*). Our method is distinctive in the following aspects: (i) We systematically investigated the whole viral genome, and we eliminated immune-evasion functions at multiple loci to obtain a safe strain that has no detectable replication in vivo; (ii) we selected mutants that induce a higher IFN response, because a transient IFN response has been shown to be essential for adaptive immunity, including the strong and diverse T cell responses; (iii) HIS virus selectively induced a transient IFN response but no other tested inflammatory responses, which reduced potential pathogenesis or side effects for future

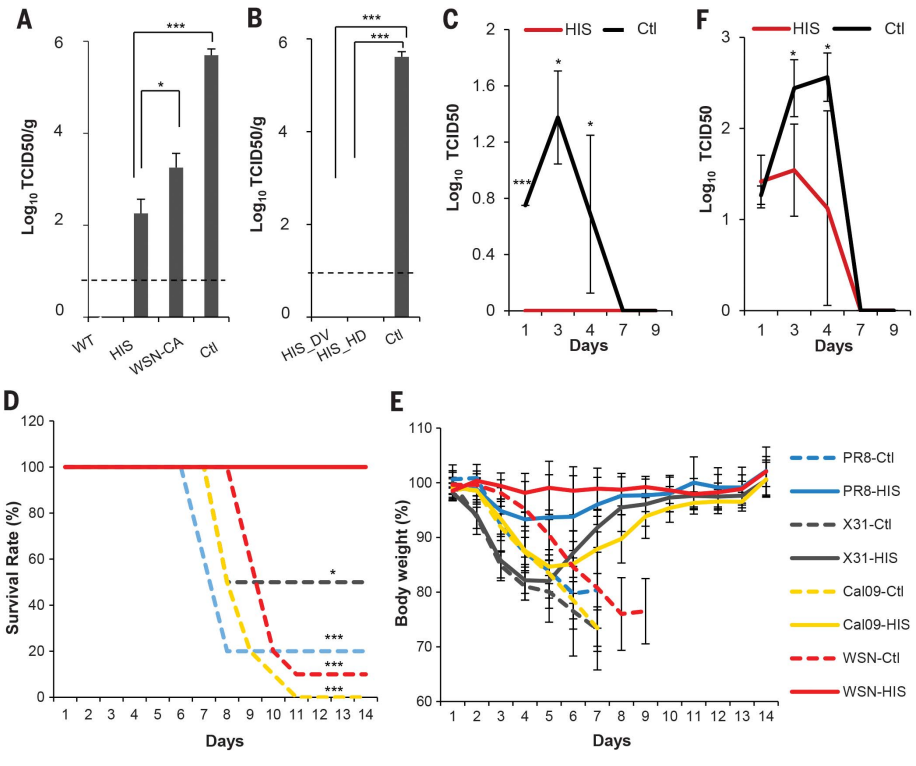

Fig. 5. HIS virus protects mice and ferrets from broad viral challenges. (**A** and **B**) Viral load in mouse lung tissues at day 2 post-challenge ($n = 4$). DV, double vaccinations with HIS virus at 1×10^4 TCID50, 28 days apart; HD, high-dose vaccination with HIS virus at 1×10^6 TCID50. Dashed lines represent detection limits. (**C**) Viral replication kinetics in ferret nasal wash after WSN virus challenge at day 35 post-vaccination ($n = 3$). (**D** and **E**) Survival rate and body weight loss of HIS-vaccinated mice after challenge with homologous and heterologous strains ($n = 10$). (**F**) Viral replication kinetics in ferret nasal wash after A/California/07/09 virus challenge at 35 days post-vaccination ($n = 3$). Error bars, SD. $^*P < 0.05$, $^{***}P < 0.001$ [ANOVA with Bonferroni multiple comparisons test for (A) and (B), two-tailed t test for (C) and (F), and log-rank test for (D)].

clinical usage. We have also applied this approach to a DNA virus and generated an effective vaccine candidate.

In general, this unbiased and quantitative high-throughput genomics system can be widely applied to other pathogens to define the impact of genome-wide mutations under certain selection conditions. Similar profiling of a viral genome can be performed with other immune components, such as cytokines, natural killer cells, or T cells, in vitro and in vivo. Inactivating additional immune evasion functions in the virus will further increase the safety and immunogenicity of its derivatives for prevention or therapy.

REFERENCES AND NOTES

1. M. T. Osterholm, N. S. Kelley, A. Sommer, E. A. Belongia, *Lancet Infect. Dis.* **12**, 36–44 (2012).
2. A. C. Tricco *et al.*, *BMC Med.* **11**, 153 (2013).
3. M. Darvishian, M. J. Bijlsma, E. Hak, E. R. van den Heuvel, *Lancet Infect. Dis.* **14**, 1228–1239 (2014).
4. A. García-Sastre, *Virus Res.* **162**, 12–18 (2011).
5. J. M. González-Navajas, J. Lee, M. David, E. Raz, *Nat. Rev. Immunol.* **12**, 125–135 (2012).
6. A. Iwasaki, P. S. Pillai, *Nat. Rev. Immunol.* **14**, 315–328 (2014).
7. J. W. Schoggins *et al.*, *Nature* **472**, 481–485 (2011).
8. J. P. Huber, J. D. Farrar, *Immunology* **132**, 466–474 (2011).
9. A. Le Bon *et al.*, *Immunity* **14**, 461–470 (2001).
10. R. M. Welsh, K. Bahl, H. D. Marshall, S. L. Urban, *PLOS Pathog.* **8**, e1002352 (2012).
11. A. Le Bon, D. F. Tough, *Curr. Opin. Immunol.* **14**, 432–436 (2002).
12. J. Crouse, U. Kalinke, A. Oxenius, *Nat. Rev. Immunol.* **15**, 231–242 (2015).
13. F. Krammer, P. Palese, *Nat. Rev. Drug Discov.* **14**, 167–182 (2015).
14. J. Talon *et al.*, *Proc. Natl. Acad. Sci. U.S.A.* **97**, 4309–4314 (2000).
15. C. Mössler *et al.*, *Vaccine* **31**, 6194–6200 (2013).
16. K. M. Graef *et al.*, *J. Virol.* **84**, 8433–8445 (2010).
17. M. Pérez-Cidoncha *et al.*, *J. Virol.* **88**, 4632–4646 (2014).
18. N. C. Wu *et al.*, *Sci. Rep.* **4**, 4942 (2014).
19. N. C. Wu *et al.*, *J. Virol.* **88**, 10157–10164 (2014).
20. E. Hoffmann, G. Neumann, Y. Kawaoka, G. Hobom, R. G. Webster, *Proc. Natl. Acad. Sci. U.S.A.* **97**, 6108–6113 (2000).
21. Y. Du *et al.*, *MBio* **7**, e01801-16 (2016).
22. N. C. Wu *et al.*, *PLOS Genet.* **11**, e1005310 (2015).
23. N. C. Wu *et al.*, *BMC Genomics* **17**, 46 (2016).
24. S. F. Elena, P. Carrasco, J.-A. Daròs, R. Sanjuán, *EMBO Rep.* **7**, 168–173 (2006).
25. E. Visher, S. E. Whitefield, J. T. McCrone, W. Fitzsimmons, A. S. Lauring, *PLOS Pathog.* **12**, e1005856 (2016).
26. B. G. Hale, R. A. Albrecht, A. García-Sastre, *Future Microbiol.* **5**, 23–41 (2010).
27. B. G. Hale, R. E. Randall, J. Ortín, D. Jackson, *J. Gen. Virol.* **89**, 2359–2376 (2008).
28. H. F. Maassab, M. L. Bryant, *Rev. Med. Virol.* **9**, 237–244 (1999).
29. H. Jin, H. Zhou, B. Lu, G. Kemble, *J. Virol.* **78**, 995–998 (2004).
30. M. J. Memoli *et al.*, *MBio* **7**, e00417–e16 (2016).
31. D. M. Carragher, D. A. Kaminski, A. Moquin, L. Hartson, T. D. Randall, *J. Immunol.* **181**, 4168–4176 (2008).
32. M. B. Doud, S. E. Hensley, J. D. Bloom, *PLOS Pathog.* **13**, e1006271 (2017).
33. S. Mueller *et al.*, *Nat. Biotechnol.* **28**, 723–726 (2010).
34. L. Si *et al.*, *Science* **354**, 1170–1173 (2016).
35. C.-Y. Wu *et al.*, *Proc. Natl. Acad. Sci. U.S.A.* **114**, 280–285 (2017).
36. L. Wang *et al.*, *Cell Host Microbe* **21**, 334–343 (2017).
37. J. Steel *et al.*, *J. Virol.* **83**, 1742–1753 (2009).
38. A. Pflug, D. Guilligay, S. Reich, S. Cusack, *Nature* **516**, 355–360 (2014).
39. S. Reich *et al.*, *Nature* **516**, 361–366 (2014).
40. S. J. Gamblin *et al.*, *Science* **303**, 1838–1842 (2004).

ACKNOWLEDGMENTS

We greatly appreciate the communication with A. te Velthuis and E. Fodor, who found that the same and similar mutations in PB2 produce mini viral RNAs (mvRNAs), which bind to RIG-I and induce IFN production. Using their method, we were able to detect these mvRNAs produced by our PB2 mutants. We thank Q. Zhou, A. York, and S. Bensinger for THP1 cells with specific gene knockouts and for discussions. We thank S. Park and S. Dubinett for the immortalized HSAECs and HBECs. Support was provided by the Whitcome Fellowship, the Burroughs Wellcome Fund, and the NIH (grants CA177322 and DE023591) to Y.D. and R.S.; the NIH (grant HL113655) to J.W.; the National Science Fund for Distinguished Young Scholars (grant 81525017) to Y. Shu; and National Science and Technology Major Project (grant 2015ZX09101044) to L.X. The sequencing data are deposited in the NIH Sequence Read Archive with accession numbers PRJNA383938, PRJNA254185, PRJNA318707, and PRJNA285135.

SUPPLEMENTARY MATERIALS

www.sciencemag.org/content/359/6373/290/suppl/DC1
Materials and Methods
Figs. S1 to S20
Tables S1 to S4
References (*41*–*70*)

1 June 2017; accepted 15 November 2017
10.1126/science.aan8806

Genome-wide identification of interferon-sensitive mutations enables influenza vaccine design

Yushen Du, Li Xin, Yuan Shi, Tian-Hao Zhang, Nicholas C. Wu, Lei Dai, Danyang Gong, Gurpreet Brar, Sara Shu, Jiadi Luo, William Reiley, Yen-Wen Tseng, Hongyan Bai, Ting-Ting Wu, Jieru Wang, Yuelong Shu and Ren Sun

Science **359** (6373), 290-296.
DOI: 10.1126/science.aan8806

Avoiding interferon avoidance

Interferon (IFN) expression is a mammal's first response to viral infection. Many viruses have thus evolved mechanisms to evade IFN. Du *et al.* developed a method to systematically ablate IFN evasion genes from live, attenuated influenza virus (see the Perspective by Teijaro and Burton). A combination of mutants was assembled to construct a virus that triggered transient IFN responses in mice but that was unable to replicate effectively. The transient IFN responses led to robust antibody and memory responses that protected against subsequent challenge with different influenza viruses. This approach could be adapted to improve other RNA virus vaccines.

Science, this issue p. 290; see also p. 277